Computers and Mathematics with Applications 62 (2011) 4068–4081

Contents lists available at SciVerse ScienceDirect

Computers and Mathematics with Applications

journal homepage: www.elsevier.com/locate/camwa

Shape optimization for tumor location

J.P. Agnelli [a,*], C. Padra [b,*], C.V. Turner [a,*]

[a] FaMAF, Universidad Nacional de Córdoba and CONICET, Córdoba, Argentina
[b] CONICET and Centro Atómico Bariloche, Bariloche, Argentina

ARTICLE INFO

Article history:
Received 25 November 2010
Received in revised form 15 July 2011
Accepted 21 September 2011

Keywords:
Bioheat transfer
Non-invasive diagnostics
Shape optimization
Gradient method

ABSTRACT

In non-invasive thermal diagnostics, accurate correlations between the thermal image at skin surface and interior human physiology are desired. In this work, an estimation methodology to determine unknown geometrical parameters of an embedded tumor is proposed. We define a functional that represents the mismatch between a measured experimental temperature profile, which may be obtained by infrared thermography on the skin surface, and the solution of an appropriate boundary problem. This functional is related to the geometrical parameters through the solution of the boundary problem, in such a way that finding the minimum of this functional form also means finding the unknown geometrical parameters of the embedded tumor. Sensitivity analysis techniques coupled with the adjoint method were considered to compute the shape derivative of the functional. Then, a nonmonotone spectral projected gradient method was implemented to solve the optimization problem of finding the optimal geometric parameters.

1. Introduction

It is well known that body temperature is an indicator of health. In general, the body surface temperature is controlled by the blood circulation underneath the skin, local metabolism, and the heat exchange between the skin and its environment [1–3]. Changes in any of these parameters can induce variations in temperature and heat flux at the skin surface reflecting the physiological state of the human body. The particular tumor architecture and angiogenesis processes can lead to an abnormal situation. Inflammation, metabolic rate, interstitial hypertension, abnormal vessel morphology and lack of response to homeostatic signals are some of the particular features that make tumors to behave differently than normal tissue in terms of heat production and dissipation. Skin temperature above a breast tumor or a malignant melanoma, a tumor of melanocytes which are found predominantly in skin, has been found to be several degrees higher than that of the surrounding area [4–7].

Therefore, the abnormal temperature on the skin surface can be used in order to predict the location and size of an embedded tumor as well as to study the tumor evolution after a treatment procedure.

Medical infrared thermography is a non-invasive and non-contact functional imaging method that measures the radiation emitted from the skin surface and provides information about subtle temperature changes in it. Medical applications of infrared thermography are not a recent phenomenon. However, in the past years their success was rather limited mainly due to the complexity, high cost, and poor sensitivity provided by the generation of infrared cameras that were available at that time. Nowadays, advances in infrared technology have again promoted its medical application as a promising non-invasive tool for imaging the functionality of superficial layers of tissues and the influence of vascular, neurogenic and metabolic processes that affect them. In [7], Santa Cruz et al. have investigated the correlation, by means of thermography, in patients treated with boron neutron capture therapy (BNCT), between the spatial extension of the acute skin reaction and the superficial dose distribution, in order to determine tolerance doses and therefore to optimize the BNCT treatment. They have also concluded that given the ability of thermography to observe the functional aspects of tissues, the

* Corresponding authors.
E-mail addresses: agnelli@famaf.unc.edu.ar (J.P. Agnelli), padra@cab.cnea.gov.ar (C. Padra), turner@famaf.unc.edu.ar (C.V. Turner).

0898-1221/$ – see front matter © 2011 Elsevier Ltd. All rights reserved.
doi:10.1016/j.camwa.2011.09.055

technique can help to locate abnormally high temperature regions as well as melanoma nodules that are virtually invisible in CT images.

The objective of this paper is the development of a methodology to estimate the location and size of an embedded (malignant melanoma) tumor region with the help of abnormal temperature profiles measured on the skin surface. We have defined a functional that represents the mismatch between a measured experimental temperature profile at the skin surface and the solution of the Pennes equation [8] with appropriate boundary conditions. This bioheat equation describes the heat transfer inside living tissues and it is widely used to solve the temperature distribution for thermal therapy [9–12]. According to literature [4–7] healthy and tumor regions have different thermal coefficient values and heat sources. We have therefore assumed that all the thermal coefficients and heat sources are piecewise constant functions. In this way we can view the location problem as a problem of finding the shape of a subdomain $\omega \subset \Omega$, using the knowledge of its (constant) density and the measurement data in some open subset of the boundary $\partial\Omega$, where Ω is the domain where the Pennes equation is considered. The optimal shape is the one that minimize the objective functional defined, and in order to find this minimum we have employed some results from the shape sensitivity analysis theory.

After we have introduced the medical facts about the skin cancer and the relation to the body temperature, the plan for the rest of this work is as follows: In Section 2 we describe the mathematical model proposed to simulate the heat transfer in a human body in 2D domains. The following section is devoted to state the inverse problem and define the functional to be minimized. Then, in Section 4 we present an introduction to the theory of sensitivity analysis and shape form derivative. In Section 5 we present the computations of the shape form derivative that allows us to compute the minimum of the functional defined in Section 3. After that, in Section 6 the results obtained from simulations with and without random noise are exposed. Moreover we compare these results with the simulations obtained using another optimization algorithm, [13]. Finally, in Section 7 some comments and conclusions are given and an Appendix is also present.

2. Mathematical model

A number of bioheat transfer equations for living tissues have been proposed since the landmark paper by Pennes appeared in 1948, [8]. The main theoretical contribution is the suggestion that the rate of heat transfer between the blood and tissue is proportional to the product of the volumetric perfusion rate and to the difference between the arterial blood temperature, and the local tissue temperature. The relationship was expressed as follows:

$$h_b = G_b \rho_b c_b (1 - \kappa)(T_b - u)$$

where h_b is the rate of heat transfer per unit volume of tissue, G_b is the perfusion rate per unit volume of tissue, ρ_b is the density of blood, c_b is the specific heat of blood, κ is a factor that accounts for incomplete thermal equilibrium between blood and tissue, T_b is the temperature of arterial blood, and u is the local tissue temperature. Although at first κ can take values in the interval $0 < \kappa < 1$, Pennes, in [8], as in most of the works related, set $\kappa = 0$. Also, he considered arterial temperature constant and equal to the body core temperature.

The proposed equation also includes a term that represents the heat transfer by conduction through the tissue and a term that represents the volumetric metabolic heat generation. These two terms coupled with the term that represents the heat transfer due to the circulation of blood give rise to the following steady-state Pennes equation:

$$-\operatorname{div}(\sigma(x)\nabla u(x)) + k(x)(u(x) - T_b) = q(x), \quad x \in \Omega \subset \mathbb{R}^n,\ n = 2, 3 \tag{1}$$

where σ is the thermal conductivity, $k = G_b \rho_b c_b$ is the perfusion coefficient, q is the metabolic heat source and T_b is the constant blood temperature. For convenience from now on we will denote $Q = q + kT_b$.

Using the fact that the thermal conductivity, the perfusion and the metabolic activity in a melanoma tumor is significantly higher than in normal tissue, we have considered that all these coefficients are piecewise continuous. For example, we can define the thermal conductivity by:

$$\sigma(x) = \begin{cases} \sigma_1, & \text{if } x \in \Omega - \overline{\omega}, \\ \sigma_0, & \text{if } x \in \omega, \end{cases} \tag{2}$$

where ω represents the tumor region and $\Omega - \overline{\omega}$ the healthy tissue (see Fig. 1). Then, if we define $u_1 = u_{|\Omega - \overline{\omega}}$ and $u_0 = u_{|\omega}$ we arrive to the following transmission problem:

$$(P) \quad \begin{cases} -\sigma_1 \Delta u_1 + k_1 u_1 = Q_1, & \text{in } \Omega - \overline{\omega}, \\ -\sigma_0 \Delta u_0 + k_0 u_0 = Q_0, & \text{in } \omega, \\ u_1 = u_0, & \text{on } \partial\omega, \\ -\sigma_1 \dfrac{\partial u_1}{\partial \eta} = -\sigma_0 \dfrac{\partial u_0}{\partial \eta}, & \text{on } \partial\omega, \\ -\sigma_1 \dfrac{\partial u_1}{\partial \eta} = \alpha(u_1 - T_a), & \text{on } \Gamma_u, \\ -\sigma_1 \dfrac{\partial u_1}{\partial \eta} = 0, & \text{on } \Gamma_l, \\ u_1 = T_b, & \text{on } \Gamma_b, \end{cases} \tag{3}$$

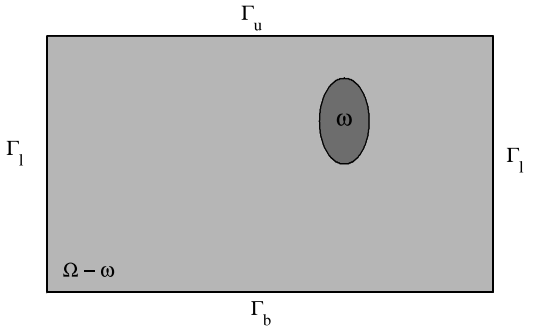

Fig. 1. Two dimensional domain. $\Omega - \overline{\omega}$ healthy tissue and ω tumor region.

where α is a heat transfer coefficient, T_a is the ambient temperature, $\Omega - \overline{\omega}$ is the domain of healthy tissue, ω is the tumor domain and η is the outward pointing unit normal. We have considered the so called transmission conditions on $\partial\omega$, whereas on $\partial\Omega$ different boundary conditions were imposed. On the bottom boundary, a constant core temperature was assumed. On the other hand, on the lateral boundaries we have adopted an adiabatic condition because we have assumed that at positions far from the center of the domain the temperature field is almost not affected by any source located near the center or any external heating or cooling. Finally, on the upper boundary a convective condition was assumed, which represents the interchange of temperature between the body and the environment.

It is possible to consider the evaporation on the skin surface, in that case we have to consider a time evolution heat equation, since the humidity coefficient depends on time.

2.1. Weak formulation of the problem

The problem described above can be formulated in a weak sense as we show below.

If we assume that u is a solution to problem (P), multiplying the partial differential equation by a function $v \in H^1(\Omega)$, integrating over Ω and using the Green formula, we obtain:

$$\int_{\Omega-\omega} (\sigma_1 \nabla u.\nabla v + k_1 uv)\, dx + \int_{\omega} (\sigma_0 \nabla u.\nabla v + k_0 uv)\, dx - \int_{\partial\Omega} \sigma_1 (\nabla u.\eta)\, d\Gamma = \int_{\Omega-\omega} Q_1 v\, dx + \int_{\omega} Q_0 v\, dx. \tag{4}$$

To simplify the notation, it is useful to define new coefficients $k(x)$ and $Q(x)$ as we have done in (2), in this way Eq. (4) can be transformed into:

$$\int_{\Omega} (\sigma \nabla u.\nabla v + kuv)\, dx - \int_{\partial\Omega} \sigma (\nabla u.\eta)\, d\Gamma = \int_{\Omega} Q v\, dx. \tag{5}$$

Since $\partial\Omega = \Gamma_b \cup \Gamma_u \cup \Gamma_l$, and using the boundary conditions, the boundary integral can be written as:

$$\int_{\partial\Omega} \sigma (\nabla u.\eta) v\, d\Gamma = -\alpha \int_{\Gamma_u} (u - T_a) v\, d\Gamma + \int_{\Gamma_b} \sigma (\nabla u.\eta) v\, d\Gamma. \tag{6}$$

The last term in the right hand side, arises because a nonhomogeneous boundary condition was imposed on Γ_b. Following the ideas in [14], we can pose our problem as we were dealing with a homogeneous Dirichlet condition. First, we define the following Hilbert space:

$$\mathcal{V}(\Omega) = \{v \in H^1(\Omega) :\ v = 0 \text{ on } \Gamma_b\}, \tag{7}$$

where the equality on Γ_b is understood in the sense of the Trace [14] and we consider the following bilinear and linear form defined by:

$$a(u, v) = \int_{\Omega} \sigma(x) \nabla u.\nabla v\, dx + \int_{\Omega} k(x) uv\, dx + \alpha \int_{\Gamma_u} uv\, d\Gamma, \tag{8}$$

$$\tilde{l}(v) = \int_{\Omega} Q(x) v\, dx + \alpha T_a \int_{\Gamma_u} v\, d\Gamma. \tag{9}$$

Next, we suppose that $u_b \in H^1(\Omega)$ is such that $u_b = T_b$ on Γ_b. Then, we obtain the weak formulation:

$$\begin{cases} \text{Find } u \in H^1(\Omega) \text{ such that} \\ u = u_b + w, \quad w \in \mathcal{V}(\Omega) \\ a(w, v) = \tilde{l}(v) - a(u_b, v), \quad \forall\, v \in \mathcal{V}(\Omega). \end{cases} \tag{10}$$

In this work, we will consider $u_b \equiv T_b$ in Ω, so we can finally write the weak formulation problem as:

$$\begin{cases} \text{Find } u \in \mathcal{V}(\Omega) \text{ such that} \\ a(u, v) = l(v), \quad \forall\, v \in \mathcal{V}(\Omega), \end{cases} \tag{11}$$

where $l(v) = \tilde{l}(v) - a(T_b, v)$. This weak formulation of the problem will be useful to compute the shape derivative of an objective functional that we will define in the next section.

3. Inverse problem

According to [4,5,7], the presence of a highly vascularized tumor can lead to the increase of local blood perfusion and the capacity of metabolic heat source and therefore this causes an increase of temperature at the skin surface. Then, the idea is to use the abnormal temperature at skin surface in order to predict the location, and size of the embedded tumor. Therefore, we have to solve the following inverse problem:

- Given constants T_b, T_a, α and a measured temperature profile u_m on the upper boundary Γ_u, find a subdomain $\omega^* \subset \Omega$ such that the solution u_{ω^*} of the boundary problem (P) with $\omega = \omega^*$ verifies $u_{\omega^*} = u_m$ on Γ_u.

The unknown ω^* is reached when the objective function:

$$\psi(\omega) = \frac{1}{2} \int_{\Gamma_u} (u(\omega) - u_m)^2 d\Gamma \tag{12}$$

vanishes, that means ψ has a minimum at ω^*.

In the next section we present the shape sensitivity analysis in order to compute the minimum of the objective functional defined above.

4. Introduction to shape sensitivity analysis

We will briefly review the most important aspect of shape sensitivity analysis.

The main objective of sensitivity analysis is to determine quality and amount of change in the behavior of a system when, in some way, a set of control variables is modified. Among many types of control possibilities, one of them is to take the geometry of the domain Ω where the system is defined as the control variable [15,16]. This case is known as shape sensitivity analysis and the typical problem is to find the shape which is optimal in such a way that it minimizes a certain objective functional while satisfying given constraints. In many cases, the functional being solved depends on the solution of a given boundary problem defined on the variable domain.

Optimization problems with constraints given by variational equations or their corresponding boundary problems arise naturally in many areas of science. For example in [17] it is considered an inverse acoustic scattering problem. The goal is to find the shape of an object immersed in an acoustic medium. The optimal shape is the one that minimizes a functional that measures the difference between the scattering signal corresponding to a trial solution and the measured scattering data available at certain locations. The scattering signal satisfies the Helmholtz equation with Sommerfeld condition imposed at infinity. In aerodynamics design problems, the objective is to find the optimal shape of a lifting surface. The cost functional in this problem depends on the flow variables at the surface of the airfoil and the flow variables are the solution of a flow problem that can be governed by the Euler or Navier–Stokes equations. In mechanics engineering the crack growth of an elastic body is viewed as a shape change and the energy release rate can be computed. The cost functional in this case is the total potential energy and the variational problem is the equilibrium equation [18,19].

What is common among all the problems mentioned above is that they can be posed as optimization problems where we search for a set of parameters, called the design or decision variables, that give the optimal value of an objective function that measures the efficiency of the system. The system is governed by a boundary-value problem called the primal problem or state equation. The variables of the primal problem are called the state variables and the objective function usually depends on them. Therefore the state equation can be seen as a constraint on the valid set of state variables that appear in the definition of the objective function. If the problem is differentiable, gradient-based algorithms can be used, and besides the value of the objective function and constraints, these methods require the calculation of their derivatives with respect to the design variables. In the next sections we show how to calculate the derivative of an objective function, when the design variable is the shape of the domain where the problem is defined.

4.1. Shape sensitivity analysis

Suppose that the system under study is governed by the following variational problem:

$$\begin{cases} \text{Find } u_\Omega \in \mathcal{W}(\Omega) \text{ such that} \\ a_\Omega(u_\Omega, v) = l_\Omega(v), \quad \forall\, v \in \mathcal{W}(\Omega), \end{cases} \tag{13}$$

where $\mathcal{W}(\Omega)$ is an appropriate Hilbert space, $a_\Omega(\cdot,\cdot)$ is a symmetric, coercive and continuous bilinear form and $l_\Omega(\cdot)$ is a continuous linear form [20]. With the subindex Ω we would like to emphasize the dependence of $a(\cdot,\cdot)$, $l(\cdot)$ and u on the domain Ω.

Assume that for this system we have a generic functional form Ψ, that depends on Ω in an explicit way and also in an implicit way through the solution of the variational problem (13). So we have

$$\psi(\Omega) := \Psi(\Omega, u_\Omega). \tag{14}$$

The goal is to find a domain Ω^* in a family $\mathcal{A}$ of admissible domains such that:

$$\psi(\Omega^*) \leq \psi(\Omega), \quad \forall\ \Omega \in \mathcal{A}. \tag{15}$$

Observe that this problem leads to the following problems: (i) the existence of an optimal domain, (ii) the characterization of the optimal domains and (iii) the construction of an algorithm to calculate one of the optimal domains. These two last problems are extremely associated with the computation of a derivative of the application:

$$\Omega \to \psi(\Omega) \in \mathbb{R}. \tag{16}$$

One difficulty in defining this derivative is that $\mathcal{A}$ has not a vectorial space structure. One way to overcome this problem is to use the method proposed originally in [21] and widely discussed by [22]. The main idea is, given a field $V : \mathbb{R}^n \to \mathbb{R}^n$, define a map from the reference domain Ω in the following way

$$x_t = p_t(x) = x + tV(x), \quad t \in \mathbb{R}^+ \tag{17}$$

where $\mathbb{R}^+ = \{t \geq 0\}$. So this approach simulates a change in shape by a known motion from an initial configuration to a deformed configuration defined by:

$$\Omega_t = \{x_t \in \mathbb{R}^n : \exists\ x \in \Omega, x_t = p_t(x)\},$$
$$\partial\Omega_t = \{x_t \in \mathbb{R}^n : \exists\ x \in \partial\Omega, x_t = p_t(x)\}.$$

In this new perturbed configuration Ω_t we have to consider a new variational equation

$$\begin{cases} \text{Find } u_{\Omega_t} \in \mathcal{W}(\Omega_t) \text{ such that} \\ a_{\Omega_t}(u_{\Omega_t}, v) = l_{\Omega_t}(v), \quad \forall v \in \mathcal{W}(\Omega_t), \end{cases} \tag{18}$$

where u_{Ω_t} is the solution in this new perturbed configuration Ω_t and the new value of the functional form is

$$\psi(\Omega_t) = \Psi(\Omega_t, u_{\Omega_t}). \tag{19}$$

Therefore the sensitivity of ψ caused by a perturbation in the system in the direction of V is

$$\begin{aligned} \dot{\psi}(\Omega; V) &= \lim_{t\to 0} \frac{\psi(\Omega_t) - \psi(\Omega)}{t} \\ &= \lim_{t\to 0} \frac{\Psi(\Omega_t, u_{\Omega_t}) - \Psi(\Omega, u)}{t}, \quad u_{\Omega_t} \in \mathcal{W}(\Omega_t),\ u \in \mathcal{W}(\Omega). \end{aligned} \tag{20}$$

It is worth noting that in the above expression the elements u and u_{Ω_t} belong to different spaces. A useful way to calculate the expression (20) is using Eq. (17) in order to transform all the expressions defined in the configuration Ω_t into the reference configuration Ω. For example, let $u_t(x) := u_{\Omega_t}(p_t(x)) = u_{\Omega_t}(x_t)$, where $u_t \in \mathcal{W}(\Omega)$ and denote the cost function by $\Psi_t(\Omega, u_t) := \Psi(\Omega_t, u_{\Omega_t}) = \psi \circ p_t(\Omega)$. Doing the same change of variables the state equation can be rewritten as:

$$\begin{cases} \text{Find } u_t \in \mathcal{W}(\Omega) \text{ such that} \\ a_t(u_t, v) = l_t(v), \quad \forall\ v \in \mathcal{W}(\Omega), \end{cases} \tag{21}$$

where $a_t : \mathcal{W}(\Omega) \times \mathcal{W}(\Omega) \to \mathbb{R}$ and $l_t : \mathcal{W}(\Omega) \to \mathbb{R}$. Finally the sensitivity of ψ caused by a perturbation in the system in the direction of V is

$$\dot{\psi}(\Omega; V) = \lim_{t\to 0} \frac{\Psi_t(\Omega, u_t) - \Psi(\Omega, u)}{t}, \quad u_t, u \in \mathcal{W}(\Omega) \tag{22}$$

if this limit exits.

4.2. A methodology to compute the shape derivative

In this section we show how to calculate the shape derivative (22) using the adjoint method.

As we showed in the previous section, the method proposed by [21] can be understood in the sense that, given a direction of perturbation V, the variable Ω is controlled uniquely by the parameter $t \in \mathbb{R}^+$. So the shape derivative of the functional Ψ in the direction V is simply defined by:

$$\dot{\psi}(\Omega; V) = \frac{d}{dt}\Psi_t(u_t)_{|_{t=0}}. \tag{23}$$

Note that we have dropped Ω in the right term of Eq. (23) because now all the expressions are defined in the reference domain Ω.

Let $u \in \mathcal{W}(\Omega)$ be fixed; we define the partial derivative of Ψ with respect to the parameter t as

$$\Psi'(u; V) = \lim_{t\to 0} \frac{\Psi_t(u) - \Psi(u)}{t} = \frac{d}{dt}\Psi_t(u)_{|_{t=0}}, \tag{24}$$

and the partial derivative of Ψ respect to u

$$\frac{\partial}{\partial u}\Psi(u; \dot{u}) = \lim_{t\to 0} \frac{\Psi(u_t) - \Psi(u)}{t} = \frac{d}{dt}\Psi(u_t)_{|_{t=0}} \tag{25}$$

where $\dot{u}$ is the material derivative that describes the variation of the response u due to the perturbation V and its given by the limit:

$$\lim_{t\to 0} \| \frac{u_t - u}{t} - \dot{u} \|_{\mathcal{W}(\Omega)} = 0. \tag{26}$$

If the derivatives Ψ', $\frac{\partial \Psi}{\partial u}$ and $\dot{u}$ exits and are Fréchet differentiable and applying the chain rule, we can rewrite the total derivative (22) as

$$\dot{\psi}(\Omega; V) = \Psi'(u; V) + \frac{\partial \Psi}{\partial u}(u; \dot{u}). \tag{27}$$

To obtain $\dot{\psi}$ we need to calculate $\dot{u}$. This can be done by differentiating the state equation with respect to t, at $t = 0$:

$$\frac{d}{dt}a_t(u_t, v; V)_{|_{t=0}} = \frac{d}{dt}l_t(v; V)_{|_{t=0}}. \tag{28}$$

In the same way as we have done with the functional form, we can define the following derivatives of the bilinear and linear form as:

$$a'(u, v; V) := \lim_{t\to 0} \frac{a_t(u, v) - a(u, v)}{t} = \frac{d}{dt}a_t(u)_{|_{t=0}}, \tag{29}$$

$$\frac{\partial a}{\partial u}(u, v; \dot{u}) := \lim_{t\to 0} \frac{a(u_t, v) - a(u, v)}{t} = a(\dot{u}, v), \tag{30}$$

$$l'(v; V) := \lim_{t\to 0} \frac{l_t(v) - l(v)}{t} = \frac{d}{dt}l_t(v)_{|_{t=0}} \tag{31}$$

and then, assuming that these derivatives are linear and continuous in the direction of the perturbation V we have that

$$\frac{d}{dt}a_t(u_t, v; V)_{|_{t=0}} = \frac{d}{dt}l_t(v; V)_{|_{t=0}}, \tag{32}$$

$$a'(u, v; V) + a(\dot{u}, v) = l'(v; V). \tag{33}$$

To avoid the calculation of $\dot{u}$, we define the following adjoint equation:

$$\begin{cases} \text{Find } \lambda \in \mathcal{W}(\Omega) \text{ such that} \\ a(\lambda, \bar{\lambda}) = -\dfrac{\partial \Psi}{\partial u}(u; \bar{\lambda}), \quad \forall \bar{\lambda} \in \mathcal{W}(\Omega). \end{cases} \tag{34}$$

The solution λ of this equation is called adjoint state. Since this equation is valid for all $\bar{\lambda} \in \mathcal{W}(\Omega)$, in particular is valid if we set $\bar{\lambda} = \dot{u}$, and using the symmetry of the bilinear form and (33), we obtain

$$-\frac{\partial \Psi}{\partial u}(u; \dot{u}) = a(\dot{u}, \lambda) = l'(\lambda; V) - a'(u, \lambda; V). \tag{35}$$

Finally, replacing this last expression in (27) we can express the total derivative of the objective functional as:

$$\dot{\psi}(\Omega; V) = \Psi'(u; V) + a'(u, \lambda; V) - l'(\lambda; V), \tag{36}$$

where λ is the solution of the adjoint problem (34). Therefore to calculate the shape derivative of the functional, using the adjoint method, we do not need to calculate $\dot{u}$, we just need to solve the state equation (13) and adjoint equation (34).

5. Computation of the shape derivative

In this section we use the results presented in the previous section and some known identities listed in the Appendix to compute the shape derivative for our particular problem.

We are interested in finding a subdomain $\omega^* \subset \Omega$, that represents the tumor region inside the body, and we assume that $\text{dist}(\partial\Omega, \omega^*) > \epsilon > 0$. Therefore we consider that $\partial\Omega$ is constant during all the process, that means $\partial\Omega_t = \partial\Omega, \forall t \in \mathbb{R}^+$, and only movements inside the domain are allowed. Then the difference between Ω and Ω_t is just the location and shape of the respective subdomains ω and ω_t. One can imagine that the domain is made of a plastic material that is fixed at the boundary but it can be deformed in the interior. For this purpose we consider V such that $\text{supp}(V) \subset \Omega$. We will give the exact definition of V in the next section.

In our problem the functional form to minimize is:

$$\psi(\omega) = \Psi(u_\omega) = \frac{1}{2}\int_{\Gamma_u} (u_\omega - u_m)^2 d\Gamma, \tag{37}$$

and represents the mismatch between a measured experimental temperature profile u_m at the skin surface and the solution u_ω of the state problem considering the domain Ω. We have denoted u_ω instead of u_Ω since Ω is fixed, therefore u depends on ω. Also, note that in this case ψ does not explicitly depend on the domain Ω, because the boundary is constant. Then, the upper boundary Γ_u is kept fixed during all the process. Therefore Eq. (36) gives

$$\dot{\psi}(\omega; V) = a'(u, \lambda; V) - l'(\lambda; V), \tag{38}$$

so we only need to compute $a'(\cdot,\cdot)$ and $l'(\lambda; V)$.

In order to transform the variational equation to the reference domain Ω, we make use of the mapping $x_t = p_t(x) = x + tV(x)$, the Jacobian $Dp_t(x) = Id + tDV(x) =: F_t(x)$ and some results listed in the Appendix, to obtain that in our case the bilineal and lineal form are given by:

$$a_t(u, v; V) = \int_\Omega [\sigma_t(\nabla u F_t^{-1}).(\nabla v F_t^{-1}) + k_t uv] \det F_t dx + \alpha \int_{\Gamma_u} uv \det F_t \|F_t^{-T}\| d\Gamma, \tag{39}$$

$$l_t(v; V) = \int_\Omega (Q_t - T_b k_t) v \det F_t dx + \alpha(T_a - T_b) \int_{\Gamma_u} v \det F_t \|F_t^{-T}\| d\Gamma. \tag{40}$$

Therefore from the definition of (29) and (31) the derivatives of these expression are:

$$a'(u, v; V) = \int_\Omega \frac{d}{dt}\{[\sigma_t(\nabla u F_t^{-1}).(\nabla v F_t^{-1}) + k_t uv] \det F_t\}_{|_{t=0}} dx + \alpha \int_{\Gamma_u} uv \frac{d}{dt}(\det F_t \|F_t^{-T}\|)_{|_{t=0}} d\Gamma, \tag{41}$$

$$l'(v; V) = \int_\Omega \frac{d}{dt}((Q_t - T_b k_t) v \det F_t)_{|_{t=0}} dx + \alpha(T_a - T_b) \int_{\Gamma_u} v \frac{d}{dt}(\det F_t \|F_t^{-T}\|)_{|_{t=0}} d\Gamma. \tag{42}$$

But from the fact that $\text{supp}(V) \subset \Omega$, we have that $\frac{d}{dt}(F_t) = DV = 0$ and $\text{div}(V) = 0$ on $\partial\Omega$, then

$$\int_{\Gamma_u} w \frac{d}{dt}(\det F_t \|F_t^{-T}\|)_{|_{t=0}} d\Gamma = 0, \quad \forall\, w(x) \in \mathcal{V}(\Omega),$$

and we obtain from the above equations:

$$a'(u, v; V) = \int_\Omega \frac{d}{dt}\{[\sigma_t(\nabla u F_t^{-1}).(\nabla v F_t^{-1}) + k_t uv] \det F_t\}_{|_{t=0}} dx, \tag{43}$$

$$l'(v; V) = \int_\Omega \frac{d}{dt}((Q_t - T_b k_t) v \det F_t)_{|_{t=0}} dx. \tag{44}$$

Now assuming that the map $p_t : \Omega \to \Omega_t$ is one to one smooth map such that $p_t^{-1}(\omega_t) = \omega_0 = \omega$ then, for example,

$$\sigma_t(x) = (\sigma_{\Omega_t} \circ p_t)(x) = \begin{cases} \sigma_0 & \text{if } x \in \omega; \\ \sigma_1 & \text{if } x \in \Omega - \omega \end{cases} \quad \forall\, t \in \mathbb{R} \geq 0,$$

where ω_0 is the original subdomain included in Ω. Therefore, the conductivity σ_t is constant with respect to the variable t and

$$\frac{d}{dt}\sigma_t = 0.$$

The same result is valid for the functions k_t and Q_t. Then expressions (43) and (44) can be rewritten as

$$a'(u, v; V) = \int_\Omega \sigma \frac{d}{dt}[(\nabla u F_t^{-1}).(\nabla v F_t^{-1}) \det F_t]_{|t=0} dx + \int_\Omega kuv \frac{d}{dt}(\det F_t)_{|t=0} dx, \tag{45}$$

$$l'(v; V) = \int_\Omega (Q - T_b k) v \frac{d}{dt}(\det F_t)_{|t=0} dx. \tag{46}$$

Finally, from the identities in the Appendix, we get that:

$$a'(u, v; V) = \int_\Omega \sigma[-(\nabla u DV).\nabla v - \nabla u.(\nabla v DV) + \nabla u.\nabla v \operatorname{div}(V)]dx + \int_\Omega kuv \operatorname{div}(V)dx, \tag{47}$$

$$l'(v; V) = \int_\Omega (Q - T_b k) v \operatorname{div}(V)dx. \tag{48}$$

Therefore, from (38), (47) and (48), the shape derivative of the functional is given by:

$$\begin{aligned}\dot{\psi}(\omega; V) = &\int_\Omega \sigma[-(\nabla u DV).\nabla \lambda - \nabla u.(\nabla \lambda DV) + \nabla u.\nabla \lambda \operatorname{div}(V)]dx \\ &+ \int_\Omega ku\lambda \operatorname{div}(V)dx - \int_\Omega (Q - T_b k)\lambda \operatorname{div}(V)dx\end{aligned} \tag{49}$$

where u is the solution of the boundary problem (P) in the reference domain and λ is the solution of the adjoint equation (34) corresponding to this problem.

6. Numerical approximation, simulations and results

6.1. Numerical approximation

In this section we discuss the numerical approximation to calculate the shape derivative using the adjoint method. We address each of the ingredients in the derivative calculation: the numerical calculation of the primal state u and the adjoint state λ, the parametrization of the subdomain ω and the definition of the vector field V.

We have considered a second order finite difference scheme, following the ideas described in [13], in order to solve the boundary problem (P) for the primal state u and the corresponding adjoint problem (34) for the adjoint state λ,

Since we are interested to localize melanoma nodules we have assumed that the tumor is a circumference in a two-dimensional domain. Therefore, to predict the location and size it was enough to determine the center and the radius of the circumference. In this way the design variables in our problem were the horizontal and vertical coordinates of the center, x_c and y_c respectively, and the radius R. From the mathematical point of view this assumption implies a reduction in the dimension of the set $\mathcal{A}$ of admissible domains where we optimize the objective functional ψ. With this assumption the set is defined by:

$$\mathcal{A} = \{\omega = B(x_c, y_c; R) : x_{\min} \le x_c \le x_{\max}, y_{\min} \le y_c \le y_{\max} \text{ and } 0 \le R \le R_{\max}\}$$

where $B(x_c, y_c; R)$ denotes the ball centered at the point (x_c, y_c) and radius equal to R.

For each design variable we have defined a particular vector field V in Ω. Although, what is common for all the fields is that they were defined by parts, adopting a certain value inside the subdomain ω and by extension outside ω. We have considered an annular extension and the field vanishes outside this region, see Fig. 2. In this way, we have that $\operatorname{supp}(V) \subset \Omega$ as we supposed in the previous section. For the design variable x_c we have considered

$$V(x, y) = \begin{cases} V_{\text{int}}(x, y) & \text{if } (x, y) \in \overline{\omega}; \\ V_{\text{ext}}(x, y) & \text{if } (x, y) \in \Omega - \overline{\omega}, \end{cases} \tag{50}$$

where $V_{\text{int}}(x, y) = (1, 0)$ for all the points inside the circumference and V_{ext} is a smooth extension. In this work we have chosen the vector field extension following the ideas presented in [23]:

$$V_{\text{ext}}(x, y) = \begin{cases} \dfrac{V_{\text{int}}(x, y)\left(\frac{w_1^p}{\operatorname{dist}((x,y),R)^\beta}\right)}{\frac{w_1^p}{\operatorname{dist}((x,y),R)^\beta} + \frac{w_2^p}{\operatorname{dist}((x,y),R_{\text{ext}})^\beta}} & \text{if } (x, y) \in \operatorname{Ann}(x_c, y_c; R, R_{\text{ext}}), \\ 0 & \text{elsewhere,} \end{cases} \tag{51}$$

where

- x_c, y_c, and R denote the coordinates of the center and radius of the actual configuration ω,
- R_{ext} is a real number to be chosen such that $0 < R < R_{\text{ext}}$,
- $\operatorname{Ann}(x_c, y_c; R, R_{\text{ext}}) = \{(x, y) : R < \operatorname{dist}((x_c, y_c), (x, y)) < R_{\text{ext}}\}$,

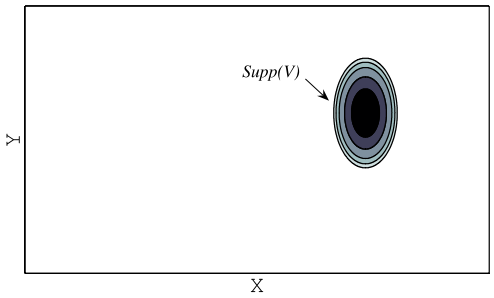

Fig. 2. The smooth vector field V_{int} defined in ω (black region) is extended to a smooth vector field V defined in all the domain Ω, such that $\text{supp}(V) \subset \Omega$.

- $\text{dist}((x, y), R)$ denotes the distance from point (x, y) to the circumference of radius R,
- $\text{dist}((x, y), R_{\text{ext}})$ denotes the distance from point (x, y) to the circumference of radius R_{ext},
- w_1, w_2 and β are parameters to be chosen.

The parameters w_1, w_2 and β, have to be chosen in order to control the smoothness of V_{ext} and which parts of the domain contribute significantly to the expression of V, see [18].

In the same way for the variable y_c we have considered the following field:

$$V(x, y) = \begin{cases} V_{\text{int}}(x, y) & \text{if } (x, y) \in \overline{\omega}; \\ V_{\text{ext}}(x, y) & \text{if } (x, y) \in \Omega - \overline{\omega}, \end{cases} \tag{52}$$

where $V_{\text{int}}(x, y) = (0, 1)$ and V_{ext} it is defined by (51). Finally for the last design variable R, the interior vector field adopted was $V_{\text{int}}(x, y) = \left(\frac{x-x_c}{R}, \frac{y-y_c}{R}\right)$ and V_{ext} was also defined by (51).

After all these considerations our problem can be rewritten in the form of the following optimization problem:

$$\begin{aligned} &\text{Minimize } \psi(x_c, y_c, R) \\ &\text{subject to } (x_c, y_c, R) \in \mathcal{C}, \end{aligned}$$

where $\mathcal{C}$ is closed convex set in $\mathbb{R}^3$ defined by

$$\mathcal{C} = \{(x, y, z) \in \mathbb{R}^3 : x_{\min} \leq x \leq x_{\max}, y_{\min} \leq y \leq y_{\max} \text{ and } z_{\min} \leq z \leq z_{\max}\}.$$

The constraint imposed by the state equation has been eliminated, using the adjoint method. In order to solve the optimization problem we have implemented a nonmonotone spectral projected gradient method on convex sets following the ideas described in [24]. The algorithm combines the projected gradient method [25] with two new features in optimization. First, it extends the typical globalization strategies associated with these methods to the nonmonotone line search scheme developed by Grippo et al. [26]. Second, it uses the spectral steplength, introduced by Barzilai and Borwein [27]. This choice of steplength requires little computational work and greatly speeds up the convergence of gradients methods.

In summary the steps required to solve the shape optimization problem are the following:

- Given an initial set of design variables $p_0 = (x_0, y_0, R_0)$:

1. *Set current design* $p = p_0$.
2. *Generate the mesh and functions* σ, k *and* Q *corresponding to the current design* p.
3. *Solve the boundary problem for the primal state* u *and adjoint state* λ.
4. *Calculate de cost function* ψ.
5. *If the stopping criteria is met, output current design as optimum design and stop, otherwise continue.*
6. *Calculate the derivatives* $\dot{\psi}(\omega; V_k)$, *for* $k = 1, 2, 3$, *and calculate the steplength* ϵ.
7. *Update* p *and go to* 2.

6.2. Simulations and results

In this part of the paper we present some simulations to show the performance of the algorithm. In all cases, the following thermal physiological parameters have been assumed [11,9,12]:

$$\begin{aligned} &\sigma_1 = 0.5 \text{ (W/m °C)}, && k_1 = 1998.1 \text{ (W/m}^3 \text{ °C)}, && Q_1 = 4200 \text{ (W/m}^3\text{)}, \\ &\sigma_2 = 0.75 \text{ (W/m °C)}, && k_2 = 7992.4 \text{ (W/m}^3 \text{ °C)}, && Q_2 = 42\,000 \text{ (W/m}^3\text{)}, \\ &T_b = 37 \text{ °C}, && T_a = 25 \text{ °C}, && \alpha = 10 \text{ (W/m}^2 \text{ °C)}. \end{aligned}$$

The dimensions of the domain Ω adopted in all the examples were 0.09×0.03 (m) and a step $h = 3 * 10^{-4}$ (m). The closed convex set $\mathcal{C}$ considered was the polyhedra $[0.02, 0.08] \times [0.01, 0.02] \times [0, 0.007]$ (m). We first show in Fig. 3(a)

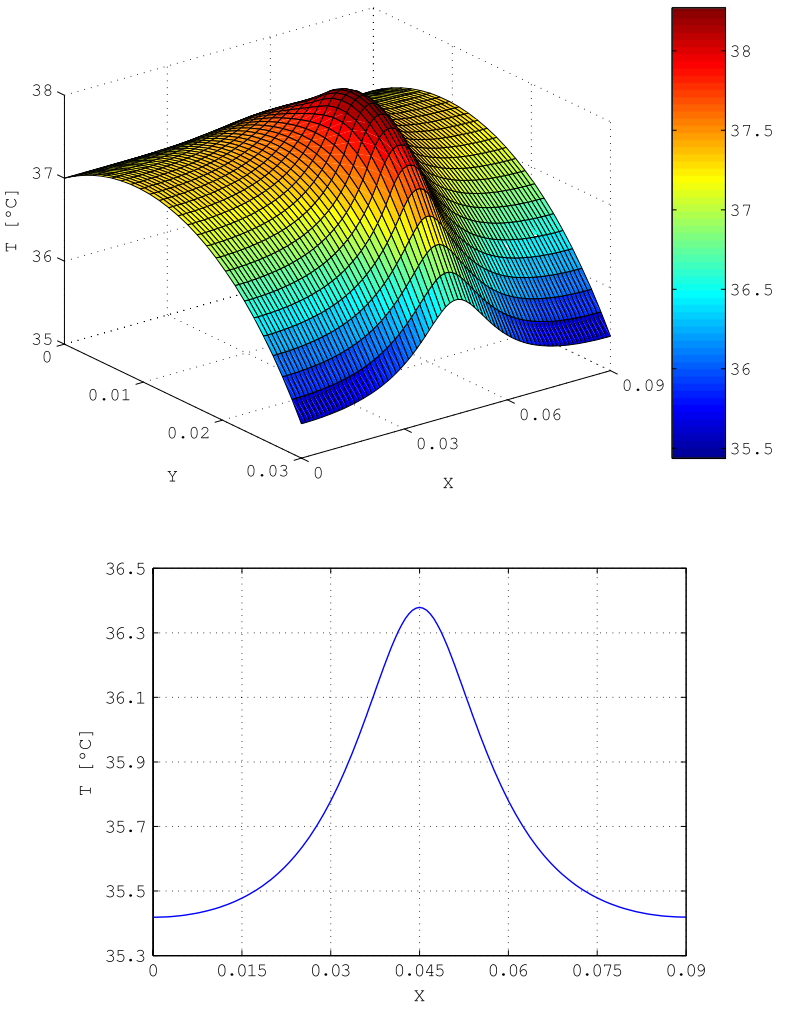

Fig. 3. (a) Temperature distribution. (b) Temperature profile on the skin surface.

the solution of the boundary problem (P) in the case when the center of the tumor was assumed at (0.045, 0.020) and the radius was 0.005 (m). We can observe the temperature distribution over the whole domain; it starts at 37 °C at the bottom and decreases, due to the convective condition at the skin surface, but it has an important increase in the region where the tumor is located. Fig. 3(b) shows the temperature profile on the skin surface, where we see a difference in temperature of almost 1 °C between the region that is above the tumor and regions that are away from it. This agrees with the idea that the presence of a highly vascularized tumor can lead to the increase of temperature at skin surface.

In Fig. 4 we show the result of the methodology proposed in the case when the center of the tumor was assumed at (0.06, 0.02) and the radius was 0.006 (m). In Fig. 4(a) the boundary of correct subdomain ω (green) and the boundary of an initial condition centered at (0.45, 0.01) with radius equal to 0.003 (m) (blue), are plotted. Fig. 4(b) shows the input data. In this case 10% of random noise was added to the input data. Finally in Fig. 4(c) we show the difference between the target subdomain and the one that has been found by the algorithm. It is clear that the computed subdomain is close to the original one. In this and the next examples the stopping criteria adopted was a tolerance on the function value $\psi < 10^{-7}$ or a maximum number of iterations equal to 500. When the input data was not contaminated with random noise the algorithms converge in almost 150 iterations in all cases.

In Fig. 5, we present another example. In this case the center of the tumor was considered at the point (0.029, 0.02) and the radius equal to 0.005 (m). Again the initial condition (blue) plotted in Fig. 5(a) was centered at the point (0.45, 0.01) and radius equals to 0.003 (m). We want to emphasize that we have run the algorithm considering different initial conditions and in all cases the results obtained were similar. Also, 10% of random noise was added to the input data. In Fig. 5(b) we can see the computed tumor using the methodology proposed here (red) and also the result obtained using the methodology proposed in [13] (black). In this last case, instead of calculating the derivative of the functional, a free derivative method called Pattern Search [28,29] was considered in order to find the optimal parameters. It is clear from the pictures that the

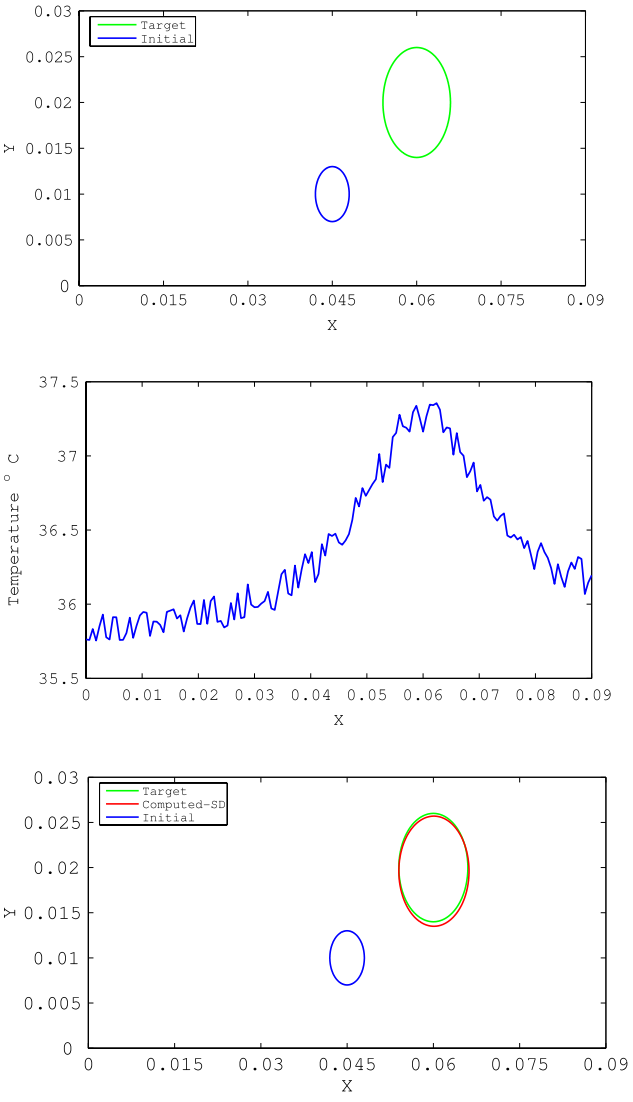

Fig. 4. (a) Initial subdomain (blue) and target subdomain (green). (b) Input data contaminated with 10% of random noise. (c) Difference between the target (green) and reconstructed subdomain (red) ω. (For interpretation of the references to colour in this figure legend, the reader is referred to the web version of this article.)

shape derivative allows us to obtain the same or even better accuracy than using the Pattern Search algorithm and also less computing time is needed. This is a consequence of the use of information obtained from the derivative of the objective functional. In Fig. 5(c) the differences between the results of the two algorithm are shown with more detail.

Finally, Table 1 shows the explicit results of the previous and other examples. In total 4 examples are presented. For each one of these examples we show the results obtained when the input data was considered without random noise and when it was contaminated with 10% of random noise. From these examples we can see that the results obtained are very accurate.

7. Conclusions and future work

Shape sensitivity analysis has been strongly related and traditionally applied to shape optimization problems in structural mechanics. However, we have shown in this paper how this approach can be used in a problem related to Medicine.

The shape derivative was calculated for the location of a tumor region using as input data the temperature profile on the skin surface that may be obtained by infrared thermography. The results presented demonstrate the feasibility of the proposed methodology. Even in the case when 10% of random noise was added to the input data the methodology showed

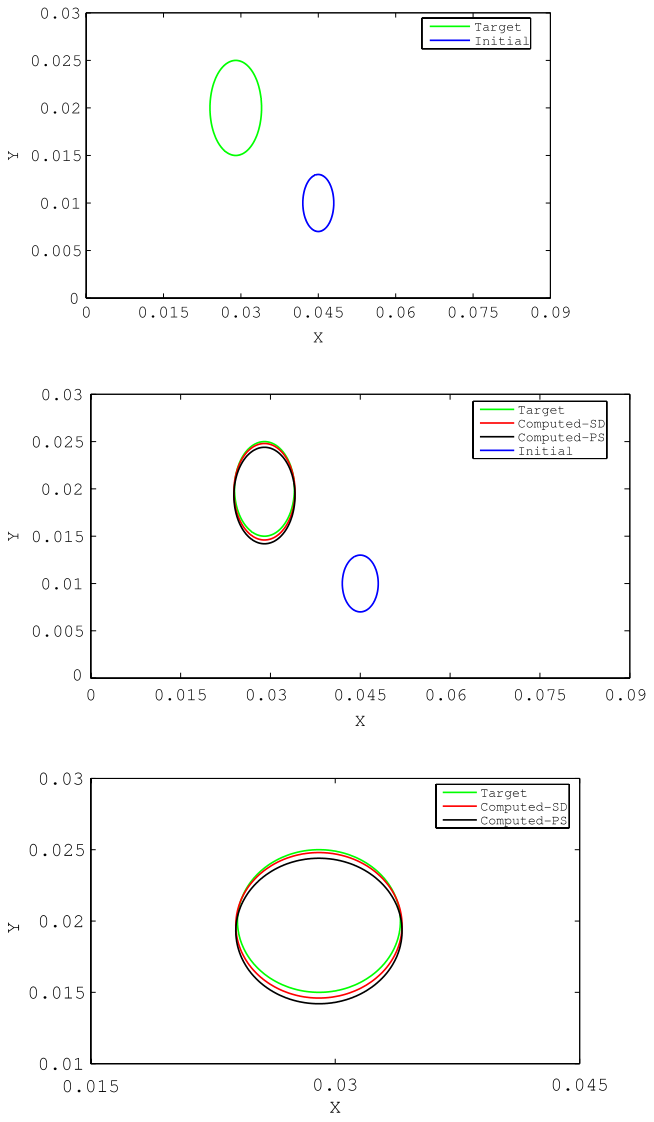

Fig. 5. (a) Initial subdomain (blue) and target subdomain (green). (b) Difference between the target and the reconstructed subdomain ω using the Shape derivative method (red) and the Pattern Search method (black). (c) Zoom of the final computation in Fig. 5(b). (For interpretation of the references to colour in this figure legend, the reader is referred to the web version of this article.)

Table 1
Estimation of the center and radius of the tumor in 2D. The different columns show the results obtained considering data without random noise and data with 10% of random noise respectively.

Original data			Without noise			10% noise		
x	y	R	x	y	R	x	y	R
0.04	0.022	0.004	0.0400	0.0218	0.0040	0.0401	0.0219	0.0039
0.029	0.02	0.005	0.0290	0.0199	0.0050	0.0290	0.0197	0.0051
0.06	0.02	0.006	0.0599	0.0199	0.0060	0.0598	0.0203	0.0059
0.07	0.016	0.007	0.0699	0.0158	0.0071	0.0701	0.0162	0.0069

a very good performance. According to this results, the methodology presented can be considered as a potential/useful tool to locate tumor regions, like melanoma nodules.

As future work we plan to consider more complex geometries in two dimensional or even in three dimensional space for the domains corresponding to the tumor and healthy tissue, taking into account the particular kind of tumor which we are dealing.

Acknowledgments

The work of the authors was partially supported by grants from CONICET, SECYT-UNC and PICT-FONCYT.

Appendix

Here we state some results that are useful in order to compute the shape derivative. The map that transforms the reference domain Ω into the perturbed Ω_t, is given by

$$x_t = p_t(x) = x + tV(x),$$

where $V(x)$ is a smooth vector field defined on an open set including Ω. This vector field describes the velocity of each point at time t. The derivative of this map with respect to the material point x is:

$$Dp_t(x) = Id + tDV(x) =: F_t(x).$$

Then, we can derive the following identities:

- $F_t^{-1} = Id - tDV + O(t^2) \Rightarrow F_{t=0} = F_{t=0}^{-1} = Id$,
- $\frac{d}{dt}(F_t) = DV$,
- $\frac{d}{dt}(F_t^{-1})_{|t=0} = -DV$,
- $\det(F_t) = \det(I + tDV) = 1 + t\ \mathrm{tr}(DV) + O(t^2) = 1 + t\ \mathrm{div}(V) + O(t)$,
- $\frac{d}{dt}\det(F_t)_{|t=0} = \ \mathrm{div}(V)$,
- $\det(F_t^{-1}) = \det(Id - tDV + O(t^2)) = 1 - t\ \mathrm{div}(V) + O(t^2)$,
- $\frac{d}{dt}(\det(F_t^{-1}))_{|t=0} = -\ \mathrm{div}(V)$,
- $dx_t = \det(F_t)dx$,
- $d\Gamma_t = \|F_t^{-T}\eta\|\ \det(F_t)d\Gamma$,
- $\frac{d}{dt}(\|F_t^{-T}\eta\|)_{|t=0} = -\eta.(DV)^T\eta$,
- $\frac{d}{dt}(\|F_t^{-T}\eta\|\ \det(F_t))_{|t=0} = -\eta.(DV)^T\eta + \ \mathrm{div}(V) =: \ \mathrm{div}_\Gamma(V)$.

References

[1] J.C. Chato, Measurement of thermal properties of biological materials, in: A. Shitzer, R.C. Eberhart (Eds.), Heat Transfer in Medicine and Biology, vol. I, Plenum Press, NY, 1985, pp. 167–173.
[2] H.F. Bowman, Estimation of tissue blood flow, in: A. Shitzer, R.C. Eberhart (Eds.), Heat Transfer in Medicine and Biology, vol. I, Plenum Press, NY, 1985, pp. 193–230.
[3] M.M. Chen, C.O. Pedersen, J.C. Chato, On the feasibility of obtaining three dimensional information from thermographic measurements, ASME Journal of Biomechanical Engineering 99 (1977) 58–64.
[4] R.N. Lawson, Implications of surface temperatures in the diagnosis of breast cancer, Canadian Medical Association Journal 75 (1956) 309–310.
[5] R.N. Lawson, M.S. Chugtai, Breast cancer and body temperatures, Canadian Medical Association Journal 88 (1963) 68–70.
[6] M. Miyakawa, J.C. Bolomey (Eds.), Non-Invasive Thermometry of the Human Body, CRC Press, Boca Raton, 1996.
[7] G.A. Santa Cruz, J. Bertotti, J. Marín, S.J. González, S. Gossio, D. Alvarez, B.M.C. Roth, P. Menéndez, M.D. Pereira, M. Albero, L. Cubau, P. Orellano, S.J. Liberman, Dynamic infrared imaging of cutaneous melanoma and normal skin in patients treated with BNCT, Appl. Radiat. Isotopes 67 (2009) s54–s58.
[8] H. Pennes, Analysis of tissue and arterial blood temperature in the resting human forearm, Journal of Applied Physiology 1 (1948) 93–122.
[9] Z. Deng, J. Liu, Mathematical modelling of temperature over skin surface and its implementation in thermal disease diagnostics, Computers in Biology and Medicine 34 (2004) 495–521.
[10] J. Liu, L.X. Xu, Boundary information based diagnostics on the thermal states of biological bodies, International Journal of Heat and Mass Transfer 43 (2000) 2827–2839.
[11] M. Paruch, E. Majchrzak, Identification of tumor region parameters using evolutionary algorithm and multiple reciprocity boundary element method, Engineering Applications of Artificial Intelligence 20 (2007) 647–655.
[12] M. Mital, E.P. Scott, Thermal detection of embedded tumors using infrared imaging, ASME Journal of Biomechanical Engineering 129 (2007) 33–39.
[13] J.P. Agnelli, A. Barrea, C.V. Turner, Tumor location and parameter estimation by thermography, Mathematical and Computer Modelling 53 (2011) 1527–1534.
[14] L.C. Evans, Partial Diffrential Equations, American Mathematical Society, 1998.
[15] M.C. Delfour, J.P. Zolesio, Shapes and Geometries: Analysis, Differential Calculus, and Optimization, Society for Industrial and Applied Mathematics, 2001.
[16] J. Sokolowski, J.P. Zolesio, Introduction to Shape Optimization: Shape Sensitivity Analysis, Springer-Verlag, Berlin, 1991.
[17] G.R. Feijóo, A.A. Oberai, P.M. Pinsky, An application of shape optimization in the solution of inverse acoustic scattering problems, Inverse Problems 20 (2004) 199–228.
[18] R.A. Feijóo, C. Padra, R. Saliba, E. Taroco, M.J. Vénere, Shape sensitivity analysis for energy release rate evaluation and its application to the study of three-dimensional cracked bodies, Computer Methods in Applied Mechanics and Engineering 188 (4) (2000) 649–664.
[19] R. Saliba, C. Padra, M.J. Vénere, E. Taroco, R.A. Feijóo, Adaptivity in linear elastic fracture mechanics based on shape sensitivity analysis, Computer Methods in Applied Mechanics and Engineering 194 (34–35) (2005) 3582–3606.

[20] D. Kinderlerer, G. Stampachia, An Introduction to Variational Inequalities and their Applications, Academic Press, New York, 1980.
[21] J. Céa, Problems of shape optimal design, in: E.J. Haug, J. Céa (Eds.), Optimization of Distributed Parameters Structures, Sijthoff and Noordhoff, Alphen, Rijn, 1981.
[22] E.J. Haug, K.K. Choi, V. Komkov, Design Sensitivity Analysis of Structural Systems, Academic Press, New York, 1986.
[23] A. Marrocco, Simulations numériques dans la fabrication des circuits a semiconducteurs, Rapport de Recheche INRIA, Rocquencourt, vol. 305, 1984.
[24] E.G. Birgin, J.M. Martinez, M. Raydan, Nonmonotone spectral projected gradient methods on convex sets, SIAM Journal on Optimization 10 (4) (2000) 1196–1211.
[25] D.P. Bertsekas, On the Goldstein–Levitin–Polyak gradient projected method, IEEE Transactions on Automatic Control 21 (1976) 174–184.
[26] L. Grippo, F. Lampariello, S. Lucidi, A nonmonotone line search technique for Newton's method, SIAM Journal on Numerical Analysis 23 (4) (1986) 707–716.
[27] J. Barzilai, J.M. Borwein, Two point step size gradient methods, IMA Journal of Numerical Analysis 8 (1) (1988) 141–148.
[28] V. Torczon, On the convergence of pattern search algorithms, SIAM Journal on Optimization 7 (1) (1997) 1–25.
[29] R.M. Lewis, V. Torczon, Pattern search methods for linearly constrained minimization, SIAM Journal on Optimization 10 (3) (2000) 917–941.